Wireless Charging Technology for Electric Vehicles Based on Efficient Magnetic Coupling Technology

Yujin Zhou[1], Jixin Wang[2*]

[1] Department of Basic Education, Shanghai Communications Polytechnic, Huilan Road No. 883, Baoshan District, Shanghai 200431, China
[2] College of Automotive Engineering, Shanghai Communications Polytechnic, Huilan Road No. 883, Baoshan District, Shanghai 200431, China
* Corresponding author, e-mail: jxwwang@outlook.com

Abstract

As the electric vehicle industry rapidly develops, the problems of cumbersome operation and insufficient anti-offset capability of traditional wired charging technology are becoming increasingly prominent. Wireless charging technology, as an innovative solution to range anxiety, has received widespread attention. To raise the performance and efficiency of wireless charging systems for electric vehicles, an improved double-layer orthogonal DD coil structure is developed, and an efficient magnetic field-coupled wireless energy transmission system based on bipolar coupling is established. Practical application denoted that the efficiency of the system reaches 92.35% at a power of 3 kW and remains at 87.64% at 9 kW. The power fluctuation rate is less than 4.30%, and the dynamic response time is shortened to 20.50 ms. Through magnetic field closed-loop control and dynamic parameter optimization, the system's environmental adaptability (operating temperature range −20~85 °C) and reliability (mean time between failures, MTBF 50,000 hours) have been improved. This study provides theoretical support and engineering practice reference for the large-scale application of wireless charging technology for electric vehicles and promotes the commercialization process of wireless charging technology.

Keywords

magnetic coupling, electric vehicles, wireless charging, DD coil, magnetic field regulation, anti offset

1 Introduction

As the electric vehicle (EV) industry rapidly develops, the issue of energy supply has become increasingly prominent (Amjad et al., 2022). Traditional wired charging relies on physical connections, which pose risks such as electrical sparks and wear and tear during insertion and removal (Tan et al., 2022). Wireless charging (WC) technology, with its advantage of non-contact energy transmission, provides innovative solutions to the problem of EV range, and has received high attention from both academia and industry (Mohamed et al., 2022). However, existing WC technologies still face two core challenges. One is the issue of transmission distance and power attenuation. Radio waves are easily affected by factors such as air medium and electromagnetic interference, resulting in a significant decrease in transmission efficiency with increasing distance (Ramakrishnan et al., 2024; Sun et al., 2025). The second issue is insufficient fault tolerance for offset. The displacement of the transmitting and receiving coils can disrupt the magnetic field coupling state, causing power fluctuations and even system detuning (Amjad et al., 2022; Pan et al., 2023).

In recent years, research on WC technology for EVs has been continuously deepening worldwide. Li et al. (2023) raised a method for simultaneously performing dynamic wireless power and data transmission to solve the mutual interference problem between wireless power and data transmission in dynamic environments. The experiment findings denoted that this method could achieve stable power output during dynamic motion. Zhang et al. (2023) raised a shared integration method based on magnetic couplers to solve the integration problem of on-board chargers and wireless power transmission systems in EVs. The experiment findings denoted that this method could achieve the sharing of wired and WC functions, with the advantages of low cost and high power density. ElGhanam et al. (2022) raised an online, mobility-based spatial EV allocation algorithm to address the coordination problem of EV charging demands in dynamic WC systems. The experiment showed that the algorithm could effectively flatten the load curve of the power grid, reduce the pressure on the power grid, and ensure that EVs obtain sufficient energy. Kumar et al. (2023) proposed

a bidirectional power transmission method to integrate EVs into the power grid, distribution network, and smart grid. The verification results of MATLAB and Simulation showed that this method could effectively integrate EVs into the power grid. Majhi et al. (2022) raised a hybrid integer optimization model to address the issue of WC being hindered by limited range, slow charging, and insufficient charging facilities along the way for EV users. The experimental results indicated that the model could provide valuable insights into the optimal settings for dynamic WC facilities in multi-route environments. Zhang et al. (2022) proposed a reconfigurable topology dual transmitting coil system to solve the problem of door to door misalignment during WC of EVs. The experiment findings denoted that the system could achieve high efficiency and stable output within the coverage area of the transmitting coil.

Although existing research has made progress in dynamic power transmission, system integration, and grid coordination, there are still shortcomings. Dynamic WC technology often focuses on optimizing a single scenario, lacking comprehensive consideration of complex road conditions and multi system coupling. The power grid coordination algorithm generally relies on high-precision positioning and real-time data interaction, without constructing a robust offline/online hybrid control mechanism, which increases the risk of system instability in the event of communication delay or data loss. Although existing integration solutions such as reconfigurable coils and mixed integer programming increase functional density, the additional topology transformation and computational overhead increase system costs. To address the aforementioned shortcomings and develop an efficient, stable, and environmentally adaptable WC system for EVs, an Efficient Magnetic Field Coupling Wireless Power Transfer Based on Bipolar (EMFC-WPT-B) system is proposed. Innovatively increasing the number of coil layers and adopting orthogonal layout have been studied to raise the anti-offset performance of DD coils. A bipolar magnetic field modulation strategy is innovatively employed to generate alternately varying pulsed magnetic fields to reduce harmonic interference and enhance the electromagnetic compatibility of the system.

2 Method

2.1 Wireless charging and magnetic coupling coil design for electric vehicles

As the EV industry quickly develops, WC technology, as an innovative way to address the issue of range, has attracted high attention from both academia and industry

(Colombo et al., 2022). At present, although WC for EVs has made some progress, it is still in the stage of continuous optimization and faces many challenges (Chittoor and Bharatiraja, 2022). To improve the WC performance, it is necessary to improve the WC system of EVs. The structure of the WC system for EVs is denoted in Fig. 1.

In Fig. 1, the WC system for EVs mainly includes a primary side, a secondary side/receiving side, and a control communication module. The primary side is composed of an inverter and a transmitting coil connected to the power grid, responsible for converting electrical energy into an alternating magnetic field. The secondary side/receiving side is equipped with a receiving coil and a rectification and filtering circuit, which are used to pick up energy from the magnetic field and convert it into usable electrical energy to charge the battery. The communication control module implements parameter monitoring and communication control of the primary and secondary sides. Magnetic coupling (MC) technology, as the core of WC, achieves efficient transmission of electrical energy and signals through one or more pairs of coupling coils. The fundamental principle underpinning MC technology is the phenomenon of electromagnetic induction. The application of an alternating current to the primary coil gives rise to the generation of an alternating magnetic field, which in turn induces an electromotive force in the secondary coil, thereby facilitating non-contact transmission of electrical energy. At present, the coil structures for WC of EVs mainly include elliptical coupling coils, solenoid coupling coils, and DD coils, as denoted in Fig. 2.

In Fig. 2, the elliptical coupling coil has strong coupling ability, but its magnetic field distribution (MFD) has certain limitations. The structure of the solenoid coupling coil is compact, but the coupling coefficient is relatively low. DD coils have good magnetic field symmetry and anti-offset ability, but there is still room for improvement. This study aims to raise the performance and efficiency of WC systems by optimizing the coil structure, to meet the requirement
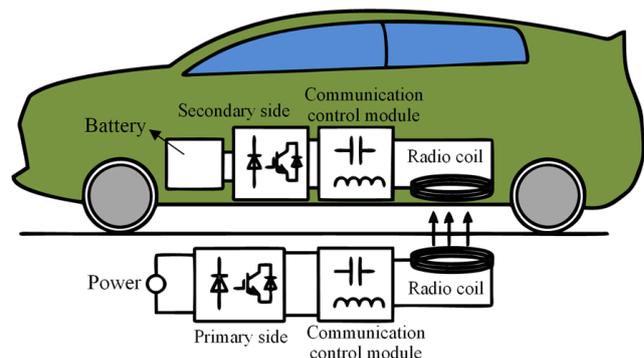

Fig. 1 Structure of wireless charging system for electric vehicles
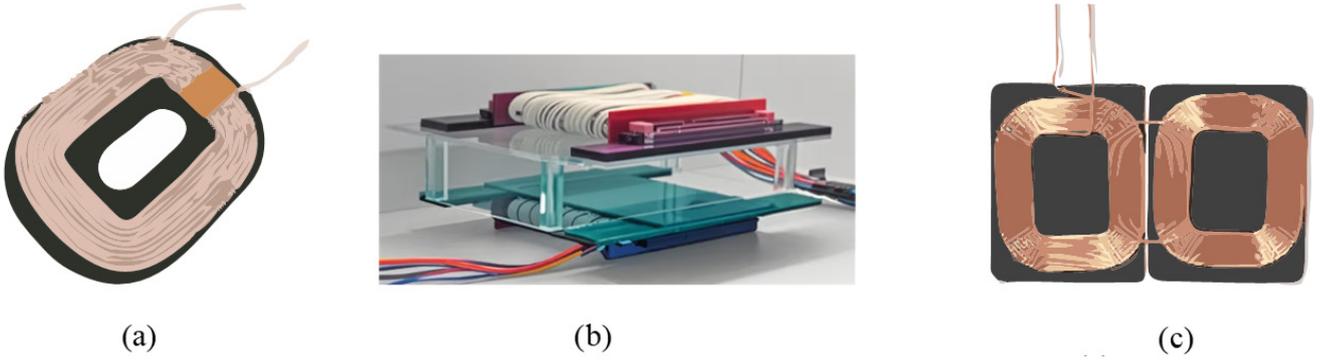
Fig. 2 Coil structures for wireless charging of electric vehicles: (a) Elliptical coupling coil; (b) Solendoid coupling coil; (c) DD coil

for WC technology in EVs. For this purpose, an Enhanced Double-layered Orthogonal DD Coil (ED-ODD) is proposed, with its structure shown in Fig. 3.

As shown in Fig. 3, ED-ODD optimizes traditional DD coils by increasing the number of coil layers and adopting an orthogonal layout. The coil consists of two layers of DD coils, one on top and one on the bottom. Each layer of DD coils is wound according to the standard DD structure, which includes two semi-circular coils and a rectangular coil for connection, forming a symmetrical and regular distribution. Two layers of coils are stacked orthogonally in space, with the plane of one layer of coils forming a 90 degree angle with the plane of the other layer of coils. This orthogonal layout makes the magnetic field interaction between coils more complex and regular. At the same time, the upper and lower layers of coils are isolated by insulating materials to prevent electrical short circuits and ensure that the two layers of coils can independently generate magnetic field interactions during operation. In addition, the lead wires of each layer of coil are respectively led out from both ends of the coil to facilitate connection to subsequent circuits (Triviño et al., 2022). The self-inductance calculation of the upper or lower coil

can be grounded on the inductance of the hollow coil, and the calculation formula is shown in Eq. (1).

$$L = \frac{\mu_0 \mu_r N^2 A}{l_m} \tag{1}$$

In Eq. (1), L hollow represents coil self-inductance, L represents vacuum magnetic permeability, μ_r means the relative magnetic permeability of the magnetic core (1 when there is no magnetic core), N represents the amount of turns in the coil, A represents the equivalent cross-sectional area of the coil, l_m represents the length of the magnetic circuit. For the coil structure with orthogonal stacking, the calculation formula for interlayer mutual inductance is shown in Eq. (2) (Duan et al., 2023).

$$M_{ud} = k_c \sqrt{L_u L_d} \tag{2}$$

In Eq. (2), M_{ud} means the mutual inductance between coil layers, k_c means the interlayer coupling coefficient, which is determined by the geometric parameters of the coil and the relative spatial position, L_u represents self-inductance of the upper coil, L_d means the self-inductance of the lower coil. This orthogonal layout ensures that the magnetic field components in two orthogonal directions satisfy the superposition principle, and the calculation formula is shown in Eq. (3) (Kamalapathi et al., 2022).

$$B_{\text{total}} = B_x e_x + B_y e_y \tag{3}$$

In Eq. (3), B_{total} represents the amount of magnetic field after superposition, B_{total} and B_y represent the magnetic field components in two orthogonal directions, respectively, e_x and e_y represent the corresponding coordinate system unit vectors, respectively. When two layers of coils work simultaneously, the formula for calculating the equivalent coupling coefficient of the WC system is denoted in Eq. (4) (Wu et al., 2023).

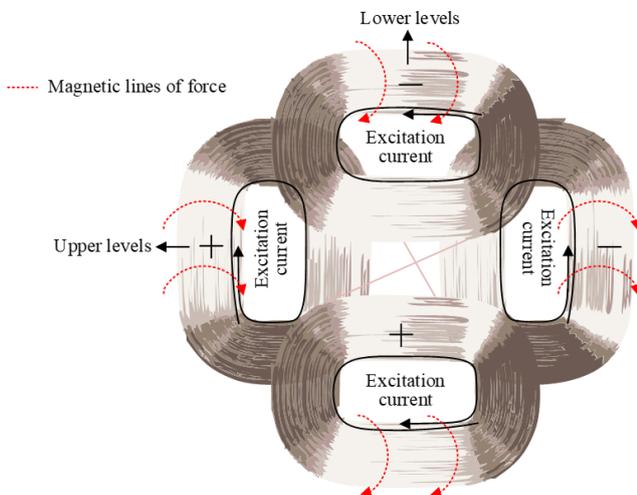$$k_{eff} = \sqrt{\frac{M_u^2 + M_d^2}{L_u L_r + L_d L_r}} \tag{4}$$

Fig. 3 ED-ODD coil structure

In Eq. (4), k_{eff} represents the equivalent coupling coefficient of the WC system, M_u represents the mutual inductance between the upper coil and the receiving coil, M_d represents the mutual inductance between the lower coil and the receiving coil, L_r represents self-inductance of the receiving coil. This structure achieves a uniform distribution of spatial magnetic fields through the superposition of orthogonal magnetic fields. Inside each coil layer, the wires are tightly and evenly wound to ensure consistent distance between each turn of the coil, to maintain the uniformity of the MFD. In the specific winding process, the condition that the wire spacing of each layer of coil needs to meet is shown in Eq. (5) (Xie et al., 2024).

$$\delta = \frac{w_c - d_w}{N - 1} \quad (5)$$

In Eq. (5), δ represents the wire spacing between each layer of coils, w_c denotes the width of the coil window, d_w means the outer diameter of the wire, δ directly affects the quality factor and proximity effect loss of the coil, and the formula for calculating the quality factor is denoted in Eq. (6).

$$Q = \frac{\omega L}{R_{ac}} \quad (6)$$

In Eq. (6), Q denotes the quality factor of the coil, ω represents the working angle frequency, R_{ac} represents communication resistance. By optimizing the coil window width w_c and magnetic core size parameters, the coupling coefficient k_{eff} can be maximized, which plays a key role in improving the system's anti offset performance.

2.2 Efficient magnetic field coupling wireless energy transmission system based on bipolarity

By increasing the number of coil layers and adopting an orthogonal layout, ED-ODD not only enhances the magnetic field strength and coupling efficiency, but also optimizes the stability of the magnetic field, providing a hardware foundation for efficient WC. However, in addition to optimizing the coil structure, an efficient power transmission method that matches it is also needed to fully leverage its performance advantages. Therefore, the study proposed the EMFC-WPT-B system. This method generates a bipolar pulse magnetic field, which alternates the direction of the magnetic field between positive and negative, thereby inducing a more stable and larger amplitude alternating electromotive force in the receiving coil to improve the efficiency and reliability of electrical energy transmission. In addition, bipolar magnetic fields can reduce harmonic interference in the system, improve electromagnetic compatibility, and further enhance the overall performance and practicality of WC systems for EVs. The structure of the EMFC-WPT-B system is denoted in Fig. 4.

As shown in Fig. 4, the EMFC-WPT-B system adopts a bipolar coupling mechanism design between the transmitting and receiving ends, which improves energy transfer efficiency and anti-offset capability by optimizing the MFD. The transmitting end of the system consists of a Direct-Current (DC) power supply, a high-frequency full bridge inverter, a dual circuit Line Compensated Converter (LCC) compensation network, and a double-layer orthogonal DD coil. The DC power supply is converted into 85 kHz high-frequency Alternating-Current (AC) power through a high-frequency inverter, and a constant amplitude excitation current is provided to the double-layer orthogonal DD transmission coil through an LCC compensation network. The orthogonal stacked double-layer DD structure can excite a spatially orthogonal distributed rotating magnetic field. The receiving end adopts an overlapping DD coil as the receiving mechanism, combined with an S-shaped compensation network and a full bridge rectification and filtering circuit. The receiving end dynamically adjusts the equivalent coupling area of the overlapping area of the receiving coils to achieve wide range load matching. The core of the MC mechanism is a combination of a double-layer orthogonal transmitting coil and a single-layer overlapping receiving coil, where the upper layer DD coil at the transmitting end is wound along the Y-axis direction, and the lower layer DD coil is arranged orthogonally along the X-axis. The transmitting end constrains the magnetic circuit through a ferrite core array, resulting in a bipolar symmetric distribution of the spatial magnetic field. The overlapping DD coil at the receiving end achieves magnetic flux path reconstruction by adjusting the overlap angle of the two D-shaped coils. The control unit of the EMFC-WPT-B system integrates a high-frequency phase-locked loop and a power factor correction module to monitor the load voltage and coupling coefficient in real time. Under lateral and longitudinal offset conditions, the magnetic field control strategy dynamically switches the working mode of the transmitting coil (single-layer excitation/double-layer orthogonal excitation) to maintain the stability of the equivalent coupling coefficient. The schematic diagram of the magnetic field controlled wireless power transmission system is denoted in Fig. 5.

As illustrated in Fig. 5, the magnetic field control of the wireless energy transmission system is achieved through closed-loop control, utilizing the double-layer orthogonal
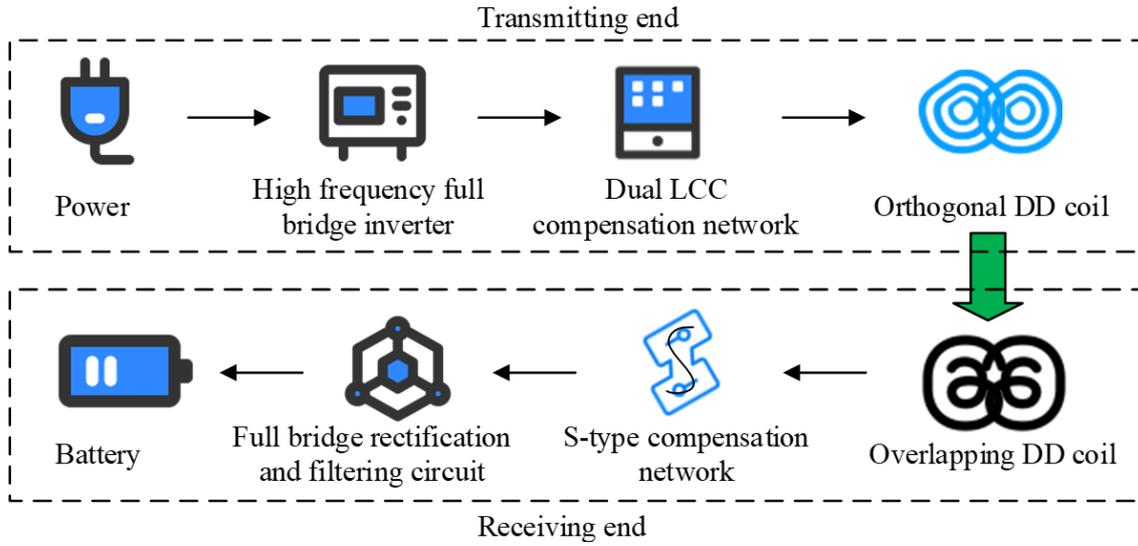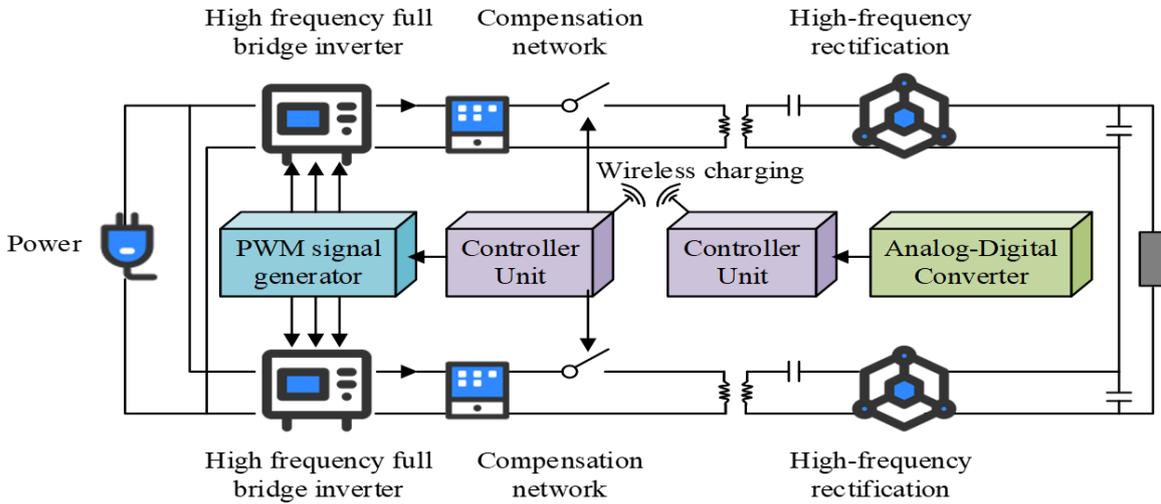
Fig. 4 Structure of EMFC-WPT-B system

Fig. 5 Schematic diagram of the magnetic field regulated wireless energy transmission system

DD receiving mechanism. The dual channel full bridge inverter drives two sets of D-shaped windings of the double-layer orthogonal DD transmitting coil, and the double-layer orthogonal DD coil at the receiving end is connected to the rectification and filtering circuit through an S-shaped compensation network. When the phase difference between the two inverters is ϕ, the calculation formula for the output current is shown in Eq. (7).

$$\begin{cases} i_1(t) = I_m \sin(\omega t) \\ i_2(t) = I_m \sin(\omega t + \phi) \end{cases}, \phi \in (0°, 180°) \tag{7}$$

In Eq. (7), ϕ represents controllable phase difference, I_m represents the amplitude of the current, I_m means the output current without phase difference, $i_2(t)$ denotes the output current when the phase difference is ϕ. The control module collects the rectified output signal in real-time and the coordinates of the receiving end, dynamically adjusts the phase

difference of the inverter drive, and excites the orthogonal D-shaped coil to generate a complementary rotating magnetic field. Magnetic field closed-loop control relies on real-time collected rectified output signals, receiver coordinates, and magnetic field intensity distribution monitored by Hall sensor arrays as feedback signals. The ferrite core guides the magnetic field to form a reconfigurable closed magnetic circuit. When the receiving end is offset, the magnetic pole pair with the largest interlocking area is automatically selected as the main transmission channel to suppress reverse magnetic flux interference, thereby achieving stable power transmission with equivalent coupling coefficient fluctuations of less than 15% within a ± 150 mm offset range. To achieve real-time optimization and regulation of parameters, the EMFC-WPT-B system is also equipped with a communication control module that monitors the parameters of the original and secondary side/receiving side and provides

feedback control to optimize the transmission process and stability. The WC process of EMFC-WPT-B system for EVs is denoted in Fig. 6.

When an EV enters the charging area, the onboard positioning system uses millimeter wave radar and ground magnetic nails to coordinate positioning, controlling the lateral deviation between the center of the receiving coil and the transmitting coil within ± 50 mm. After the vehicle comes to a complete stop, the primary control unit performs handshake authentication with the in-vehicle Battery Management System (BMS) through the Bluetooth Low Energy communication module to obtain the State of Charge (SoC) status, rated voltage, and maximum allowable charging current parameters of the battery. The system self-test program immediately starts, sequentially detecting key parameters such as the temperature of the inverter Insulated Gate Bipolar Transistor, LCC compensation capacitor withstand voltage value, and ferrite core temperature rise, and measuring the spatial magnetic field intensity distribution through a Hall sensor array. The magnetic field safety criterion is shown in Eq. (8).

$$B_{max} \leq B_{limit} \tag{8}$$

In Eq. (8), B_{max} represents the spatial magnetic field strength, $B_{limit}=6.25\mu T$. After safety verification, the secondary S-shaped compensation network dynamically adjusts the resonant capacitor based on the real-time coupling coefficient to maintain resonance. The original dual channel full bridge inverter injects 85 kHz high-frequency current into the double-layer orthogonal DD transmitting coil to form an adjustable rotating magnetic field.

Fig. 6 Wireless charging process of EMFC-WPT-B system for electric vehicles

During charging, the primary monitoring unit collects data, while the secondary monitoring unit monitors power and efficiency. The data is exchanged through a 2.4 GHz module. When the offset exceeds 100 mm, the control module calculates the optimal phase combination based on the magnetic field model and reconstructs the magnetic field path. The system performs dynamic efficiency optimization every 5 seconds, adjusts the inverter duty cycle, and ensures that the efficiency is ≥ 85% when the coupling coefficient fluctuates. The charging termination condition is intelligently determined by the BMS based on the battery voltage curve. After reaching the preset SoC threshold, the system executes a soft shutdown program. The output current of the inverter decreases linearly with a slope of 10 A/ms, while the secondary discharge resistor is connected to the circuit to absorb residual energy, ultimately completing the physical separation of the electronic lock of the charging connector and generating a charging metering bill.

3 Results
3.1 Performance analysis of the ED-ODD coil
To analyze the performance of ED-ODD, an experimental platform was set up for the study. The experimental platform consisted of a high-frequency inverter power supply, a bipolar coupling mechanism, a digital control module, a multi-channel data acquisition system, and a programmable electronic load. The experimental platform adopted a full bridge inverter topology and drove a double-layer orthogonal DD transmission coil through a dual LCC compensation network. The receiving end was equipped with double-layer orthogonal DD coils and S-shaped compensation capacitors with the same structure. The original and secondary side/receiving side achieved parameter interaction through a 2.4 GHz wireless communication module. The magnetic field strength was monitored in real-time by a Hall sensor array, the offset was calibrated by a laser rangefinder, and the system parameters were synchronously collected and recorded by a LabVIEW upper computer. The experimental platform's parameters are outlined in Table 1.

The double-layer orthogonal DD coil is composed of two layers of standard DD structure coils stacked orthogonally, with each layer containing two semi-circular arcs and connecting rectangles, forming a regular symmetrical distribution. The ED-ODD coil size of this study is 300 mm × 300 mm, with a wire diameter of American Wire Gauge 18 Leeds wire. The number of turns is calculated according to the inductance formula to ensure self-inductance of
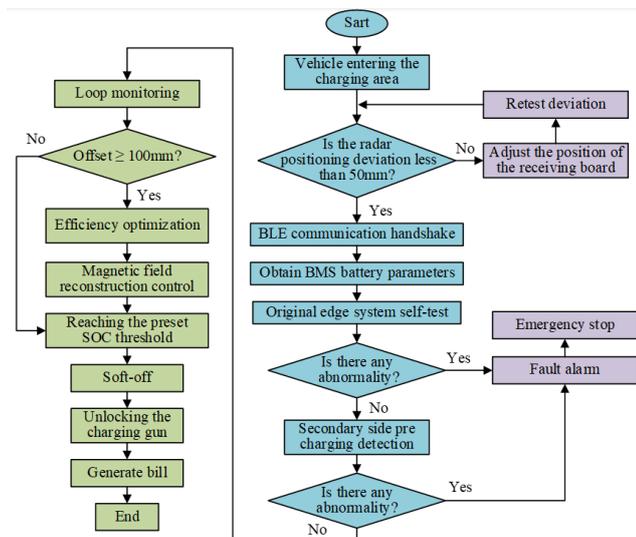
Table 1 Experimental platform parameters

Parameter category	Technical specifications/configuration	Test equipment model	Remarks
High-frequency Inverter power supply	Input voltage: 380 V DC ± 5%	TesTech PA3000 power analyzer	Full-bridge topology, SiC MOSFET
	Switching frequency: 85 kHz ± 1%		Duty cycle adjustment range: 0.2~0.8
Coupling mechanism	Coil dimensions: 300 mm×300 mm	Agilent 4294A impedance analyzer	Litz wire, AWG18
	Ferrite core thickness: 5 mm		Relative permeability is 2,000
	Self-inductance: =350 μH, =320 μH	Maxwell FEM simulation platform	Primary LCC / Secondary S compensation
Control module	Positioning accuracy: ± 50 mm	Keysight N6705C DC power supply	Millimeter-wave radar + magnetic nail positioning
	Communication module: Wi-Fi + BLE 5.0		Control cycle: 5 ms
Detection module	Voltage measurement accuracy: ± 0.5%	NI PXIe-6363 DAQ Card	Sampling rate: 250 kS/s
	Current measurement bandwidth: 100 kHz		Hall sensor: HX-10 Series
	Temperature monitoring range: −40 °C~125 °C		PT1000 temperature probe
	Magnetic field resolution: 0.1 μT		Triaxial magnetic field sensor
Load module	Power range: 0~3 kW	Chroma 63200A electronic load	CV/CC Mode switchable
	Bleeder resistor: 10 Ω ± 5%		Power margin: 200%
	Cooling method: Forced air cooling		Heat sink temperature ≤ 80 °C

350 μH and 320 μH, respectively. The coil spacing is determined by the window width and wire diameter according to the formula to ensure the uniformity of the magnetic field. Insulating materials isolate the upper and lower layers to prevent short circuits and enhance system safety and stability. The study used an elliptical coupled coil (Ellipse) and a DD coil (DD) for comparison. The transmission distance was 200 mm (fixed air gap), the input voltage was 380 V DC, the switching frequency was 85 kHz, and the offset direction was transverse (along the X-axis). To ensure fairness in comparison, the traditional DD coil uses a Leeds wire winding with a wire diameter of AWG18, and the number of turns is calculated using an inductance formula to achieve similar self-inductance under the same testing conditions as ED-ODD. It uses a ferrite core with a relative magnetic permeability of 2,000 and a size of 300 mm × 300 mm. The elliptical coil also uses AWG18 Leeds wire, with the number of turns determined according to experimental requirements to ensure comparison with other coils under the same input and output conditions. The magnetic core material is consistent with the DD coil, and the size is set according to common elliptical coupling coil specifications. The long and short axis sizes are suitable for the experimental platform space and magnetic field distribution testing requirements. The changes in coupling coefficient and transmission efficiency of each coil under different offsets are shown in Fig. 7.

In Fig. 7 (a), the coupling coefficient of ED-ODD was consistently significantly higher than that of traditional DD coils and Ellipse within the lateral offset range of 0–150 mm. For example, in the absence of offset, ED-ODD was 0.25, which was 13.63% and 38.88% higher than DD coil (0.22) and Ellipse (0.18), respectively. When the offset increased to 150 mm, the ED-ODD was 0.14, which was still 1.75 times that of the DD coil (0.08) and 7 times that of the Ellipse (0.02). This indicates that the double-layer orthogonal magnetic field structure of ED-ODD effectively expands the magnetic field coverage range. In Fig. 7 (b), the transmission efficiency of ED-ODD was superior to that of the comparative coil within the range of 0-150 mm offset. For example, at 0 offset, ED-ODD was 92.30%, which was 3.8 percentage points higher than DD coil (88.50%) and 6.4 percentage points higher than Ellipse (82.10%). When the offset increased to 150 mm, the ED-ODD was 78.50%, still 11 percentage points higher than the DD coil (67.50%) and 25.3 percentage points higher than the Ellipse (53.20%). This is because the high coupling coefficient of ED-ODD reduces leakage losses, while its orthogonal magnetic field design reduces eddy currents and skin effects, thereby improving energy transfer efficiency. It can be seen that ED-ODD is significantly superior to traditional DD and Ellipse in terms of anti-offset performance and energy transfer efficiency. The changes in leakage flux intensity and temperature rise of each coil under different offsets are shown in Fig. 8.
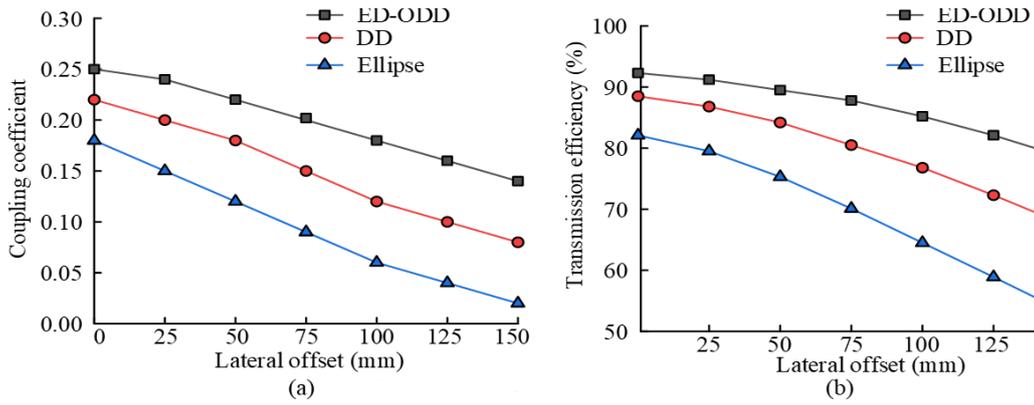
Fig. 7 Changes in coupling coefficient and transmission efficiency of each coil: (a) Coupling coefficient; (b) Transmission efficiency

In Fig. 8 (a), the leakage flux intensity of ED-ODD was significantly lower than that of DD and Ellipse within the range of 0-150 mm offset. For example, without offset, the ED-ODD was 4.20 μT, which was only 61.76% of the DD coil (6.80 μT) and 44.21% of the Ellipse (9.50 μT). When offset to 150 mm, ED-ODD was 8.00 μT, which was still lower than DD (13.50 μT) and Ellipse (19.10 μT). This is because the double-layer orthogonal magnetic field of ED-ODD forms a closed loop, and the reverse magnetic field component offsets some of the leakage magnetic field. In Fig. 8 (b), the temperature rise of ED-ODD was always the lowest. For example, when there was no offset, the temperature rise was 12.50 °C, which was 4.3 °C and 9.7 °C lower than DD (16.80 °C) and Ellipse (22.30 °C), respectively. When offset to 150 mm, the temperature rise of ED-ODD was 22.80 °C, which was still lower than DD (33.80 °C) and Ellipse (42.10 °C). This is because the high coupling coefficient of ED-ODD reduces reactive current and eddy current losses, while the lower leakage flux reduces Joule heating of coil resistance. DD and Ellipse require higher current to maintain power due to low coupling and high leakage flux, resulting in increased copper and iron losses. It can be seen

that ED-ODD performs excellently in leakage suppression and temperature rise control, providing a reliable technical foundation for high power density and low electromagnetic radiation wireless power transmission systems.

3.2 Performance and practical application effect analysis of the EMFC-WPT-B system

The study optimized the traditional DD coil by increasing the number of coil layers and adopting orthogonal layout, resulting in higher coupling coefficient, transmission efficiency, and anti-offset performance of ED-ODD. At the same time, it performed well in leakage suppression and temperature rise control. To verify the effectiveness of the EMFC-WPT-B system and its effectiveness in practical applications, the system was studied and applied in a certain automotive company. The comparison methods are Strongly Coupled vehicle-to-vehicle (V2V) system and Loosely Coupled V2V system. The actual positioning of each system during auxiliary vehicle charging is shown in Fig. 9.

As shown in Fig. 9 (a), in the Strongly Coupled V2V system, the deviation between the actual position and the ideal position was relatively small, and most of the data points
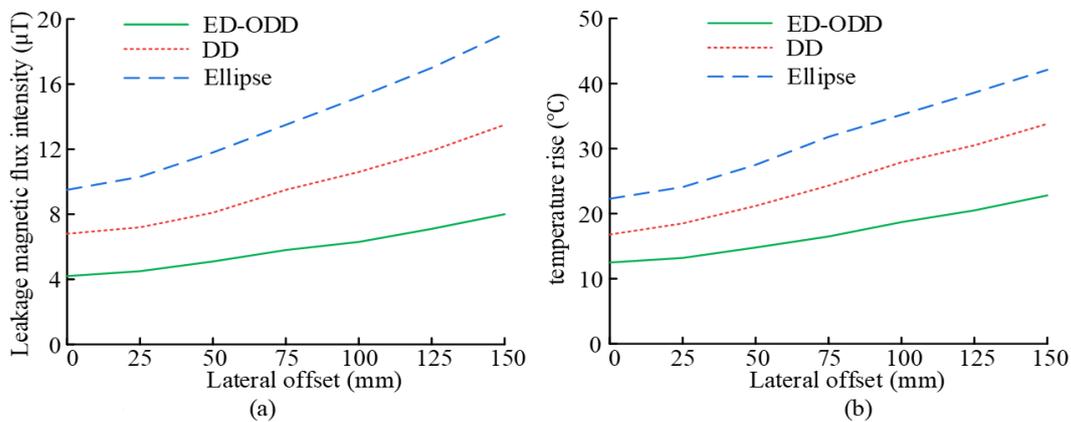

Fig. 8 Leakage flux intensity and temperature changes of each coil: (a) Leakage magnetic flux intensity; (b) Temperature changes

were distributed within ± 2 mm around the ideal position, indicating that its high magnetic field coupling characteristics can effectively constrain the displacement of the receiving end. As shown in Fig. 9 (b), the actual position distribution range of the Loosely Coupled V2V system expanded, reflecting the decrease in positioning accuracy caused by the divergence of MFD under low coupling degree. In Fig. 9 (c), the actual position of the EMFC-WPT-B system almost completely coincided with the ideal position, verifying its accurate closed-loop positioning capability. The EMFC-WPT-B system performed better due to its double-layer orthogonal DD coil structure, which optimized the uniformity of magnetic field spatial distribution and reduced the interference of magnetic field distortion on positioning accuracy. The transmission efficiency and power fluctuation of each system under different charging powers are shown in Fig. 10.

According to Fig. 10 (a), EMFC-WPT-B had the highest transmission efficiency (92.35%) at 3 kW, and the transmission efficiency decreased the least with increasing power (still maintaining 87.64% at 9 kW). The transmission efficiency of Strongly Coupled V2V was moderate, while Loosely Coupled V2V had the lowest transmission efficiency, and the transmission efficiency decreased significantly at high power (66.85% at 9 kW). In Fig. 10 (b), the power fluctuation rate increased with the increase of power, but the EMFC-WPT-B fluctuation rate was always the lowest. For example, at 9 kW, it was 4.30%, which was lower than Strongly Coupled V2V (7.85%) and Loosely Coupled V2V (4.30%). The comprehensive performance advantage of the EMFC-WPT-B system comes from the combination of MFD optimization and intelligent dynamic control, which enables it to balance efficient transmission and stability in high-power scenarios. In other aspects, the actual performance of the EMFC-WPT-B system is denoted in Table 2.
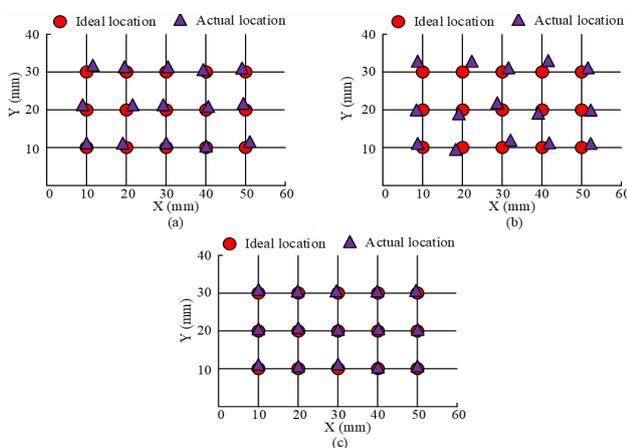

Fig. 9 Actual positioning of the car during charging: (a) strongly coupled V2V; (b) loosely coupled V2V; (c) EMFC-WPT-B

According to Table 2, the mean time between failures (MTBF) is 50,000 hours based on the IEC 62305 reliability testing standard. Through accelerated aging tests with temperature cycling (−20~85 °C), humidity cycling (10%~95% RH), and vibration testing (10~2,000Hz), the test duration conversion meets the industry's accelerated life assessment standards. EMFC-WPT-B performed best at extreme temperatures (−20~85 °C) and humidity (10~95%), with a significantly wider operating range than Strongly Coupled V2V (−10~70 °C) and Loosely Coupled V2V (0~50 °C). ANOVA analysis denoted significant differences between groups ($p < 0.05$). The mean time between failures (50,000 h) of EMFC-WPT-B far exceeded that of the control group. Weibull distribution fitting (β=1.8) showed that its failure mode was more stable, and its anti-delamination strength (9.85 MPa) increased by more than 58% compared to other systems (t=18.7, $p < 0.001$). The insulation strength (12.5 kV/mm) and electrostatic immunity (± 15 kV) of EMFC-WPT-B reached the highest level, and one-way analysis of variance (F=45.6, $p < 0.001$) verified that its safety was significantly better than that of the control group. The radiation emission limit of EMFC-WPT-B (30.15dB μV/m) met the CISPR 11 Class B standard, and covariance analysis (F=32.1, $p < 0.001$) showed that its frequency band optimization effectively suppressed interference. EMFC-WPT-B achieved comprehensive performance of high reliability, low radiation, and fast response under complex working conditions through material optimization, intelligent control, and standard compatibility design.

4 Conclusion

This study addressed the issues of low coupling efficiency and insufficient anti-offset capability in WC systems for EVs. An ED-ODD coil structure was proposed, and an EMFC-WPT-B system was developed by combining bipolar magnetic field modulation strategy. Experiments showed that the coupling coefficient of ED-ODD reached 0.14 when laterally offset by 150 mm, which was 1.75 times higher than that of traditional DD coils (0.08). The transmission efficiency was 78.50% at the same offset, which was 11 percentage points higher than the traditional DD coil (67.50%). The EMFC-WPT-B system achieved an efficiency of 92.35% at a power of 3 kW and still maintained 87.64% at 9 kW. The mean time between failures of EMFC-WPT-B was 50,000 hours, which was 66.67% higher than that of Strongly Coupled V2V (30,000 hours). Existing technologies such as Li's dynamic energy transmission focus on a single scenario, Zhang's shared integration increases topology
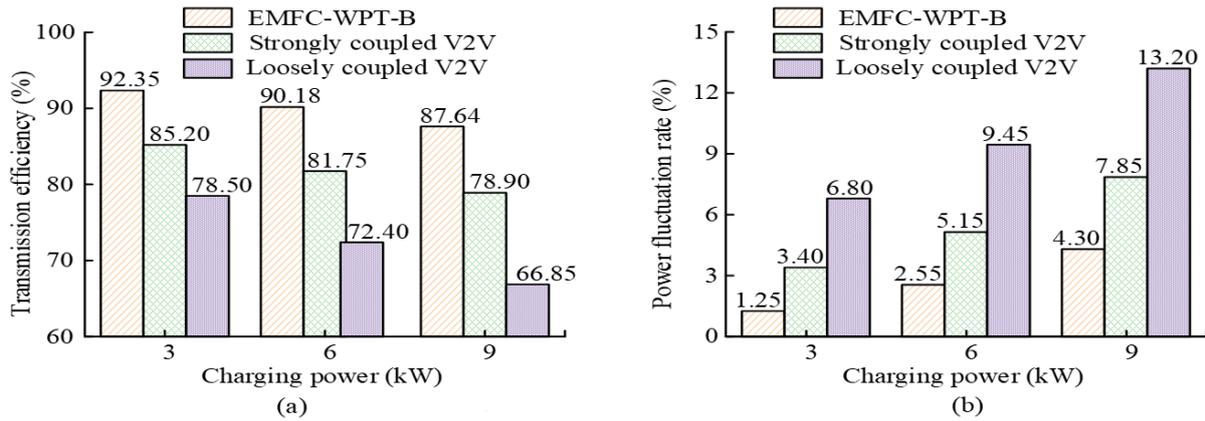
Fig. 10 Transmission efficiency and power fluctuation of each system under different charging powers: (a) Transmission efficiency; (b) Power fluctuation

Table 2 Comprehensive performance indicators of EMFC-WPT-B system

Performance category	Metric	EMFC-WPT-B	Strongly coupled V2V	Loosely coupled V2V	Statistical analysis
Environmental adaptability	Operating temperature range (°C)	−20~85	−10 ~ 70	0~50	Sample size $n = 50$, 95% confidence interval, $p < 0.05$
	Humidity range (%)	10~95	20~85	30~80	ANOVA showed significant inter-group differences ($F = 6.32$, $p = 0.002$)
Reliability	Mean time between failures (hours)	50,000 ± 1,200	30,000 ± 900	10,000 ± 600	Weibull distribution fitting ($\beta = 1.8$, $\eta = 52,300$)
	Delamination resistance (MPa)	9.85 ± 0.15	6.20 ± 0.30	3.45 ± 0.25	Independent t-test ($t = 18.7$, $p < 0.001$)
Safety	Insulation strength (kV/mm)	12.50 ± 0.25	8.75 ± 0.35	5.20 ± 0.40	One-way ANOVA ($F = 45.6$, $p < 0.001$)
	ESD immunity (kV)	± 15 (Class A)	± 8 (Class B)	± 4 (Class C)	Rank-sum test showed higher immunity ($Z = 4.8$, $p < 0.001$)
EMC performance	Radiated emission limit (dB μV/m)	30.15 ± 1.20 (CISPR 11)	42.50 ± 2.50	55.80 ± 3.80	Covariance analysis ($F = 32.1$, $p < 0.001$, frequency as covariate)
	Conducted disturbance suppression rate (%)	92.35 ± 0.75	78.60 ± 1.20	65.40 ± 1.80	Regression analysis showed negative correlation with frequency ($R2 = 0.89$)
Other performance	Dynamic response time (ms)	20.50 ± 0.85	55.30 ± 2.10	120.80 ± 5.50	Repeated-measures ANOVA ($p < 0.001$)
	Shielding effectiveness (dB)	45.20 ± 1.50	30.80 ± 2.00	18.60 ± 2.50	Significant material-structure interaction ($F = 24.3$, $p < 0.001$)

costs, and ElGhanam's power grid coordination relies on high-precision positioning. Compared to existing technologies, this research method has significant advantages. The EMFC-WPT-B system achieves efficient energy transfer and stability in high-power scenarios by optimizing MFD and intelligent dynamic control. Its double-layer orthogonal DD coil structure optimized the uniformity of magnetic field spatial distribution, reduced the interference of magnetic field distortion on positioning accuracy, and thus demonstrated excellent anti-offset performance in practical applications. However, this study still has certain limitations.

The optimization of coil structure mainly focuses on the adaptability of lateral offset, longitudinal offset, and multi angle offset, which needs further research. The impact of vehicle movement on MFD during dynamic charging was not taken into account. In the future, more new coil topologies will be explored to enhance multidimensional offset adaptability. Vehicle-pile cooperative dynamic charging models need to be constructed to enable stable energy transfer in mobile states; system costs need to be reduced and integration needs to be improved to facilitate large-scale commercialization of the technology.

References

Amjad, M., Farooq-i-Azam, M., Ni, Q., Dong, M., Ansari, E. A. (2022) "Wireless charging systems for electric vehicles", Renewable and Sustainable Energy Reviews, 167, 112730.
https://doi.org/10.1016/j.rser.2022.112730

Chittoor, P. K., Bharatiraja, C. (2022) "Wireless-Sensor Communication Based Wireless-Charging Coil Positioning System for UAVs With Maximum Power Point Tracking", IEEE Sensors Journal, 22(8), pp. 8175–8182.
https://doi.org/10.1109/JSEN.2022.3156089

Colombo, C. G., Miraftabzadeh, S. M., Saldarini, A., Longo, M., Brenna, M., Yaici, W. (2022) "Literature Review on Wireless Charging Technologies: Future Trend for Electric Vehicle?", In: 2022 Second International Conference on Sustainable Mobility Applications, Renewables and Technology (SMART), Cassino, Italy, pp. 1–5. ISBN 978-1-6654-7147-3
https://doi.org/10.1109/SMART55236.2022.9990331

Duan, Z., Hu, C., Liu, W., Liu, J., Chu, Z., Yang, W., Li, L., Shen, G. (2023) "An All-MXene-Based Flexible, Seamless System with Integrated Wireless Charging Coil, Micro-Supercapacitor, and Photodetector", Advanced Materials Technologies, 8(15), pp. 2300157–2300158.
https://doi.org/10.1002/admt.202300157

ElGhanam, E., Sharf, H., Odeh, Y., Hassan, M. S., Osman, A. H. (2022) "On the Coordination of Charging Demand of Electric Vehicles in a Network of Dynamic Wireless Charging Systems", IEEE Access, 10, pp. 62879–62892.
https://doi.org/10.1109/ACCESS.2022.3182700

Kamalapathi, K., Nayak, P. R. N., Tyagi, V. K. (2022) "Development and analysis of three-coil wireless charging system for electric vehicles", International Journal of Circuit Theory and Applications, 50, pp. 249–271.
https://doi.org/10.1002/cta.3158

Kumar, A., Joshi, B. P., Sagar, A., Kumar, N., Bertoluzzo, M., Singh, A. (2023) "Opportunities and Challenges for Electric Vehicle Wireless Charging with Home", In: 2023 International Conference on Power Energy, Environment & Intelligent Control (PEEIC), Greater Noida, India, pp. 221–225. ISBN 979-8-3503-5777-6
https://doi.org/10.1109/PEEIC59336.2023.10451967

Li, X., Zheng, F., Wang, H., Sun, Y., Dai, X., Hu, J. (2024) "A Simultaneous Power and Data Transfer Method for Dynamic Wireless Charging Electric Vehicles", IEEE Journal of Emerging and Selected Topics in Power Electronics, 12(1), pp. 328–340.
https://doi.org/10.1109/JESTPE.2023.3323473

Majhi, R. C., Ranjitkar, P., Sheng, M. (2022) "Optimal allocation of dynamic wireless charging facility for electric vehicles", Transportation Research Part D: Transport and Environment, 111, 103461.
https://doi.org/10.1016/j.trd.2022.103461

Mohamed, N., Aymen, F., Alharbi, T. E. A., El-Bayeh, C. Z., Lassaad, S., Ghoneim, S. S. M., Eicker, U. (2022) "A Comprehensive Analysis of Wireless Charging Systems for Electric Vehicles", IEEE Access, 10, pp. 43865–43881.
https://doi.org/10.1109/ACCESS.2022.3168727

Pan, W., Liu, C., Tang, H., Zhuang, Y., Zhang, Y. (2024) "An Interoperable Electric Vehicle Wireless Charging System Based on Mutually Spliced Double-D Coil", IEEE Transactions on Power Electronics, 39(3), pp. 3864–3872.
https://doi.org/10.1109/TPEL.2023.3344663

Ramakrishnan, V., Savio, D. A., Balaji, C., Rajamanickam, N., Kotb, H., Elrashidi, A., Nureldeen, W. (2024) "A Comprehensive Review on Efficiency Enhancement of Wireless Charging System for the Electric Vehicles Applications", IEEE Access, 12, pp. 46967–46994.
https://doi.org/10.1109/ACCESS.2024.3378303

Sun, H., Ma, X., Hu, R. Q., Christensen, R. (2025) "Precise coil alignment for dynamic wireless charging of electric vehicles with rfid sensing", IEEE Wireless Communications, 32(1), pp. 182–189.
https://doi.org/10.1109/MWC.004.2300593

Tan, Z., Liu, F., Chan, H. K., Gao, H. O. (2022) "Transportation systems management considering dynamic wireless charging electric vehicles: Review and prospects", Transportation Research Part E: Logistics and Transportation Review, 163, 102761.
https://doi.org/10.1016/j.tre.2022.102761

Triviño, A., Sánchez, J., Delgado, A. (2022) "Efficient Methodology of the Coil Design for a Dynamic Wireless Charger", IEEE Access, 10, pp. 83368–83378.
https://doi.org/10.1109/ACCESS.2022.3196023

Wu, Z., Zhao, Y., Zhang, N. (2023) "A Literature Survey of Green and Low-Carbon Economics Using Natural Experiment Approaches in Top Field Journal", Green and Low-Carbon Economy, 1(1), pp. 2–14.
https://doi.org/10.47852/bonviewGLCE3202827

Xie, R., Wu, Y., Tang, H., Zhuang, Y., Zhang, Y. (2024) "A Strongly Coupled Vehicle-to-Vehicle Wireless Charging System for Emergency Charging Purposes With Constant-Current and Constant-Voltage Charging Capabilities", IEEE Transactions on Power Electronics, 39(4), pp. 3985–3989.
https://doi.org/10.1109/TPEL.2024.3352909

Zhang, Y., Pan, W., Wang, H., Shen, Z., Wu, Y., Dong, J., Mao, X. (2022) "Misalignment-Tolerant Dual-Transmitter Electric Vehicle Wireless Charging System With Reconfigurable Topologies", IEEE Transactions on Power Electronics, 37(8), pp. 8816–8819.
https://doi.org/10.1109/TPEL.2022.3160868

Zhang, Y., Wu, Y., Shen, Z., Pan, W., Wang, H., Dong, J., Mao, X., Liu, X. (2023) "Integration of Onboard Charger and Wireless Charging System For Electric Vehicles With Shared Coupler, Compensation, and Rectifier", IEEE Transactions on Industrial Electronics, 70(7), pp. 7511–7514.
https://doi.org/10.1109/TIE.2022.3204857